ORIGINAL PAPER

Phosphane-stabilized gold clusters: investigation of the stability of $[Au_{13}(PMe_2Ph)_{10}Cl_2]^{3+}$

Jia Li · Shu-Guang Wang

Abstract The phosphane-stabilized gold cluster $[Au_{13}(PMe_2Ph)_{10}Cl_2]^{3+}$ was studied using density functional theory. The extraordinary stability of the cluster has been attributed to the stability of the gold core and the protection conferred by ligands. Here, five stability factors of the gold core were explained and verified by investigating the Au_{13}^{5+} core in detail. Interactions between the gold core and several PR_3 ligands (R = Me, H, I, Br, Cl, F) were investigated according to the different electron donor abilities of each ligand; bonding energy between the ligand and the gold core was found to increase with the electronegativity of the R substituent. Furthermore, two other aspects of the ligands were clarified: how the ligand stabilizes the Au_{13}^{5+} core, and which kind of ligand provides the best stabilization for the cluster.

Keywords Stability · Gold clusters · Density functional theory

Introduction

Ligand-stabilized gold clusters have been extensively investigated due to their unique physicochemical properties and applications such as optical response [1], catalysis [2], chemical sensing [3] and magnetism [4]. It is often necessary to obtain well-defined cluster samples whose properties can be "tuned" through chemical modification for use in fundamental or applied research. In a number of cases it has now been shown that, through careful choice of the stabilizing ligands and/or reaction conditions, one can produce clusters tailored to possess desired properties.

Phosphanes (PR_3) belong to the most ubiquitous ligands in transition-metal chemistry. Typically, PR_3 may be attached as weak Lewis base ligands that coordinate to the gold cluster surface through dative bonds. The PR_3 ligand not only provides complete steric protection of the cluster surface, but also stabilizes the cluster by changing its electron configuration as an electron donor ligand. Besides being applied in academic research, gold clusters with phosphane ligands have been used as powerful catalysts in industrially important homolytically catalyzed chemical reactions. Another important area where PR_3–gold complexes have been applied is in the biochemistry of gold-based medicinal agents [5].

Typical examples of gold clusters with phosphane ligands include $Au_{11}(PAr_3)_7X_3$ [6], $[Au_{11}(PPh_3)_8]X^{2+}$ [7], $[Au_{11}(BINAP)_4X_2]^+$ [8], $[Au_{13}(PMe_2Ph)_{10}Cl_2]^{3+}$ [9], $[Au_{20}(PPh_3)_8]^{2+}$ [10], $[Au_{39}(PPh_3)_{14}Cl_6]^{2+}$ [11], and $Au_{55}(PPh_3)_{12}Cl_6$ [12]. All of these clusters have a remarkably large HOMO–LUMO (highest occupied molecular orbital–lowest unoccupied molecular orbital) energy gap, suggesting that they would be highly chemically inert. It is the extraordinary stability of gold clusters that gives them their crucial character, and which has led to their extensive application. However, the factors governing the stability of gold clusters remain largely unknown. The few theoretical research studies that have been performed [13–19] have mostly been to investigate geometrical structure or to confirm experimental observations. Any investigation into the stability of gold clusters needs to focus on two separate aspects: (1) the stability of the gold core itself, and (2) the effect of ligands on gold core stability.

J. Li · S.-G. Wang (✉)
School of Chemistry and Chemical Technology,
Shanghai Jiao Tong University,
Shanghai 200240, China
e-mail: sgwang@sjtu.edu.cn

Some recent experimental studies have reported a few metal clusters with unusual stability, such as WAu_{12} [20], $AlPb_{12}^+$ [21], $CuSn_{12}^-$ [22] and so on. Most of these clusters satisfy five primary rules of stability:

1. Compact, symmetrical geometrical structure: there is a maximum degree of ligand binding for each atom, with no special active point having a compact, symmetric geometrical structure. For example, most M_{13} (M = transition metal) cores tend to be more stable in I_h or O_h symmetry [20–25].

2. Particularly efficient radial bonding: a metal cage will create particularly efficient radial bonding by embedding an atom in the center of the cage [26, 27]. Also, there will be specific effects on cage stabilization if the embedded atom has an appropriate radius and electronic shell.

3. Filled spherical electronic shells with major energy gap to vacant orbital: the stable metal cluster can be described by a "noble-gas superatom" analogy with a large HOMO–LUMO gap. Analogous to atomic theory, all the valence electrons of the metal core disperse the delocalized "superatomic orbitals" [28, 29]. Thus, the exceptional stability is associated with a special total count of valence electrons, corresponding to strong electron shell closures in an anharmonic mean-field potential.

4. Aurophilic attraction in the periphery: one common and rather specific property of monovalent gold compounds is their tendency to form clusters of Au(I) species. This is now commonly attributed to unusually strong d^{10}–cd^{10} interactions [30]. It turns out that the optimized peripheral Au–Au distances here are short, about 280 pm. At this distance, two Au(I) centers would feel a mutual van der Waals (vdW) attraction of roughly up to 100 kJ mol^{-1} per pair [31].

5. Strong relativistic effects: it is now well known that the very specific properties of gold are determined to a significant extent by the strong relativistic effects on its 5d and 6 s valence shells [32].

However, even these five factors are still not enough to stabilize naked gold clusters because of the strong aggregation effect of small clusters. Thus, in practice, naked gold clusters need the complete steric protection and the electronic stabilization conferred by the protection of ligands. Besides PR_3 ligands, other ligands, such as Cl^-, may counteract the positive charge of gold cores.

In this paper, quantum chemical calculations of the geometries and bond dissociation energies in $[Au_{13}(PMe_2Ph)_{10}Cl_2]^{3+}$ were carried out using density functional theory (DFT). We explained the five stability factors of gold cores noted above by investigating the Au_{13}^{5+} core. Lastly, comparing different ligands, we investigated two other ligand effects with regards to cluster stabilization: (1) how does the ligand stabilize the gold core in detail, and (2) which kind of ligand confers the best stabilization on the gold cluster.

Calculational details

All calculations of geometry optimization were carried out using the TURBOMOLE package of ab initio quantum chemistry programs [33]. Interactions between the gold core and the ligand were determined by energy decomposition analysis (EDA), which was used to analyze bonding using the ADF2007 program [34].

Besides Hartree-Fock (HF), Møller-Plesset (MP) and coupled cluster (CC) approaches, the following density

Table 1 Au_2, AuH, AuCl and AuCu: comparison of Møller-Plesset (MP), coupled cluster (CC), and several density functional (DF) approaches results (TZVPP basis), deviations (Δ) of calculated bond distances R_e (in pm) and bond energies D_e (in eV) from the experimental values[a]

	ΔMP2	ΔCC2	ΔXα	ΔS-V	ΔVBP	ΔPBE	ΔB3L	ΔHF	Experimental [58–60]
Au_2									
R_e	+ 0.9	+ 0.4	+ 4.4	+ 1.4	+ 7.4	+ 7.7	+ 9.9	+ 15.2	247.2
D_e	−0.26	−0.09	+ 0.14	+ 0.49	−0.16	−0.10	−0.42	−1.62	2.29
AuH									
R_e	−2.9	−2.1	+ 2.3	+ 0.5	+ 1.6	+ 1.6	+ 2.1	+ 5.0	152.4
D_e	−0.41	−0.28	−0.40	+ 0.37	−0.09	−0.24	−0.36	−1.76	3.36
AuCl									
R_e	+ 1.5	+ 2.0	+ 3.6	+ 1.1	+ 6.3	+ 6.0	+ 8.2	+ 12.4	219.9
D_e	−1.05	−0.88	−0.54	−0.14	−0.74	−0.65	−0.23	−2.04	3.54
AuCu									
R_e	+ 2.8	+ 0.6	+ 1.6	−1.3	+ 4.4	+ 4.8	+ 7.3	+ 16.3	233.0
D_e	−0.06	+ 0.21	+ 0.27	+ 0.71	+ 0.09	+ 0.14	−0.19	−1.48	2.34
$\overline{|\Delta R|}$	2.0	1.3	3.0	1.1	4.9	5.0	6.9	12.2	
$\overline{|\Delta D|}$	0.44	0.37	0.34	0.43	0.27	0.28	0.30	1.73	

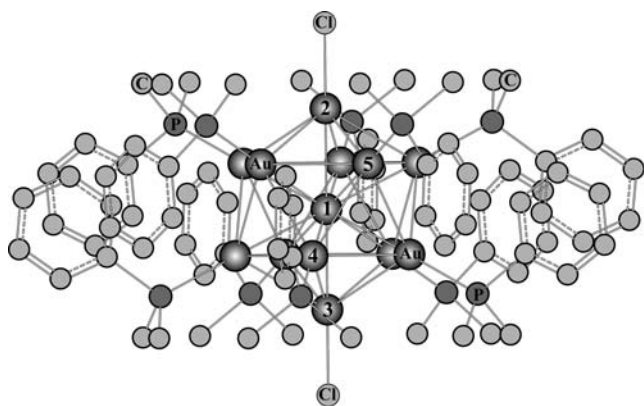[a] $\overline{|\Delta X|}$: average absolute deviation from experimental values, $X = R_e, D_e$

Fig. 1 Optimized structure of $[Au_{13}(PMe_2Ph)_{10}Cl_2]^{3+}$ (H atoms are omitted)

functional (DF) exchange-correlation approaches were tested on the present compounds: Slater's local exchange potential (Xα) [35] without, and with Vosko-Wilk-Nusair's [36] local correlation (S–V), and with the non-local exchange-correlation corrections of Becke and Perdew (VBP) [37, 38], or of Perdew-Burke-Ernzerhof (PBE) [39], and Becke's three parameter hybrid of HF and Lee-Yang-Parr's potential (B3L) [40, 41]. The MP2 and CC2 calculations were performed with the help of the resolution-of-identity (RI) approximation for the two-electron part. The triple-ζ valence-quality plus two polarizations (TZVPP) or one polarization (TZVP) basis from the TURBOMOLE basis set library, respectively, were used for the Au atom and the other atoms in all calculations, along with a default 60-electron relativistic effective core potential (ECP) [42] for the Au atom. The counter-poise correction (CPC) to the basis set superposition error (BSSE) of the finite basis sets turned out to be small here, of the order of 0.03 eV.

With the ADF2007 program, the local spin density (LSD) approximation [43] with the correlation correction of Vosko et al. (VWN) and the gradient corrections to exchange and correlation developed by Perdew and Wang (PW91) [44] were used. Scalar relativistic effects were considered at the level of the zero-order regular approximation (ZORA) [45]. Slater-type-orbital (STO) basis sets of triple-zeta plus double polarization quality (TZ2P) were used for all atoms [46]. The small inner core shells up to 4f were calculated by the Dirac method [47] and kept frozen for all 6-row metal elements; the 5 s, 5p, 5d and 6 s shells were treated as valence shells.

For further elucidation, a natural bond orbital (NBO) analysis was performed (PW91-DFT level, SDD [42] and 6–31 g* [48] basis sets for the metal and the other atoms, respectively) using Gaussian03 [49].

Results and discussion

Before investigating the gold cluster, test calculations were carried out on the experimentally and theoretically well-defined Au_2, AuH, AuCl and AuCu (Table 1). These small molecules are bonded by a two-center σ_g orbital, strongly stabilized by relativistic effects. Without any correlation correction of the orbital interaction (HF), the bond is seriously too weak and too long. Ab initio non-variational correlation corrections (CC, MP) are not completely satisfactory, at least with conventional basis sets without r_{12} functions. The two local DF approximations (LDA: Xα and S–V) actually give reasonable bond distances and bond energies. Gradient-corrected (GGA: VBP and PBE) and B3L approaches overestimate the bond length by 5–10 pm, while the energies are still reasonable. Thus, in this paper, S–V was applied to geometry optimization.

Optimized structure of $[Au_{13}(PMe_2Ph)_{10}Cl_2]^{3+}$

Optimized structure of the cluster is shown in Fig. 1. The cluster has D_{5d} symmetry structure and can be fractionalized into two subsystems: (1) a Au_{13}^{5+} core, and (2) a closed shell composed of ten PMe_2Ph ligands and two Cl^- ligands. The core has an approximate I_h symmetry structure. Each of the 12 surface atoms of the core is bound directly to one PMe_2Ph or Cl^- ligand. In the experimental work of Mingos and colleagues [9], it is suggested that the two Cls are "para" relative to each other. We calculated the three isomers: "para", "ortho" and "meta"; the "para" isomer has the lowest energy because of repulsion of the same electronic charge.

Table 2 shows the geometric parameters of $[Au_{13}(PMe_2Ph)_{10}Cl_2](PF_6)_3$. In the calculations used in this work, HF and a few DF exchange-correlation approaches were tested on the present complex. Compared with experimental results, VBP, B3L and HF approaches overestimate the bond length by 10–15 pm, while LDA (S–V) can, on the whole, reproduce the structure.

Table 2 Main geometric parameters of $[Au_{13}(PMe_2Ph)_{10}Cl_2]^{3+}$ as calculated by several different functions, compared with experimental parameters (in pm and deg)[a]

[a] Sequence number of Au atom is shown in Fig. 1

	$R_{Au(1)–Au(2)}$	$R_{Au(1)–Au(5)}$	$R_{Au(4)–Au(5)}$	$R_{Au–Cl}$	$R_{Au–P}$	$\theta_{P–Au(5)–Au(1)}$
HF	286.2	303.6	317.1	242.3	250.7	176.1
B3L	281.1	295.6	308.8	238.6	243.0	176.7
VBP	277.8	290.4	302.6	236.8	239.9	177.0
S–V	271.4	278.8	291.6	230.5	231.1	178.7
Experimental	271.6	278.9				178.0

Table 3 Total energies (E_{tot}), zero-point energies (ZPE), HOMO–LUMO gap (Gap_{H-L}), numbers of imaginary frequency (NIMAG), and relative energies (E_{rel}; with ZPE correction) of various possible isomers of Au_{13}^{5+} (in eV)

	Symmetry	E_{tot}	ZPE	Gap_{H-L}	NIMAG	E_{rel}
1	I_h	−47,893.319	0.134	2.080	0	0
2	O_h	−47,893.257	0.142	1.423	0	0.070
3	D_{5h}	−47,893.260	0.146	1.717	1	0.071
4	D_{6h}	−47,891.996	0.138	0.681	12	1.327
5	D_{6d}	−47,892.232	0.118	0.425	8	1.071
6	C_{2V}	−47,893.246	0.139	1.378	1	0.078

Stability of the Au_{13}^{5+} core

As shown in Fig. 1, the Au_{13} core has an approximate I_h symmetry structure. In the I_h symmetrical structure, the core has the maximum degree of ligand binding for each atom, and has no specific active point compared to other symmetries. The icosahedral molecule WAu_{12} was predicted by Pyykkö and Runebreg [23] and produced experimentally by the group of Lai-Sheng Wang [20]. Comparing the electronic structure of WAu_{12}, Au_{13} needs five positive charges to be in agreement with the appropriate "aufbau" rule of delocalized superatomic orbitals. Around the 18e of Au_{13}^{5+}, the peripheral gold atoms contribute one electron $6s^1$ while the central gold atom also contributes its d-electrons, which participate strongly in bonding. In the icosahedral case, the angular momenta $l=0$, 1 and 2 for the spherical cluster, or the central-atom s, p and d orbitals, span the irreducible representations a_g, t_{1u} and h_g, respectively. The '18 electrons' occupy the $\left(a_g = s\right)^2 \left(t_{1u} = p\right)^6 \left(h_g = d\right)^{10}$ at the occupied valence band. In addition, there is an electron shell closing the gold core with a large HOMO–LUMO gap.

As we know, the stability of lead clusters is determined by the interplay between geometrical (close-packed) and electronic (closed shell) structural features. For Au_{13}^{5+} clusters, we optimized various possible isomers of Au_{13}^{5+} to investigate this feature. Frequency analyses determined the nature of the stationary points. The results of computation (Table 3) show that the I_h symmetrical Au_{13}^{5+} is the most stable isomer. It is 0.07 eV lower in energy than the second best isomer O_h, which is one of the two isomers without imaginary frequency. The extremely large HOMO–LUMO gap of about 2.08 eV is striking. The exceptionally large HOMO–LUMO gaps of the highly symmetric I_h suggest very favorable stable electronic structures.

We next investigated the orbitals of Au^+, Au_{12}^{4+} and Au_{13}^{5+} in detail. Figure 2 is the energy-level correlation diagram of the frontier orbitals of Au^+, Au_{12}^{4+} and Au_{13}^{5+}. The orbitals reveal the degree to which the valence electrons of the constituent atoms in Au_{13}^{5+} are delocalized. It can be seen that most of the orbital interactions are contributed by the vacant $6s$ and $6p$ orbitals of Au^+ and the occupied $4t_{1u}$ and $3a_g$ orbitals of Au_{12}^{4+}. At the same time, the results of NBO

analysis prove that the electronic configuration of the central gold atom is $6s^{1.17}5d^{9.90}6p^{0.54}$, suggesting that the vacant $6s$ and $6p$ orbitals of Au^+ gain many electrons from the orbital interaction. In addition, there is much electrostatic interaction between the central gold atom (with a charge of −0.72) and the 12 cage gold atoms (with a charge of +0.48). So the central gold atom contributes to the particularly efficient radial interaction to stabilize the cluster.

In addition, the electronic configuration of the peripheral gold atoms is $6s^{0.59}5d^{9.88}6p^{0.05}$. The peripheral gold atoms contribute one electron $6s^1$ and form the Au(I) units that are formally charged 1+. However, the Au(I)–Au(I) attraction does not resemble the pure closed shell interaction of d^{10}–d^{10}. From the electronic configuration, we know that there are 0.12 holes in the Au5d shell, 0.59 electrons in Au6s, and 0.05 electrons in Au6p. So the Au(I)–Au(I) attraction also comprises a covalent interaction via Au $5d$–$6s$–$6p$ hybridization.

The $[Au_{13}(PH_3)_{10}Cl_2]^{3+}$ Dewar-Chatt-Duncanson model

The Au_{13}^{5+} is isoelectronic with WAu_{12}, but strongly expanded due to Coulomb repulsion. The distances between the central atom and peripheral atoms are 274.4 and
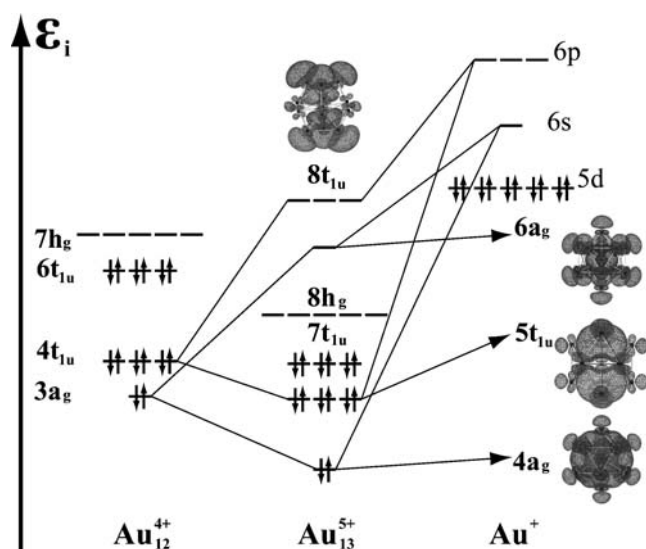

Fig. 2 Orbital correlation diagrams of Au_{12}^{4+}, Au^+ and Au_{13}^{5+}

Table 4 Main geometric parameters of $[Au_{13}(PR_3)_{10}Cl_2]^{3+}$ (PR_3 = PMe$_2$Ph, PMe$_3$, PH$_3$, PF$_3$), $Au_{13}Cl_2^{3+}$ and Au_{13}^{5+} (in pm), and HOMO–LUMO gap (Gap$_{H-L}$) of complexes (in eV)[a]

	$R_{Au(1)-Au(2)}$	$R_{Au(1)-Au(5)}$	$R_{Au(4)-Au(5)}$	R_{Au-Cl}	R_{Au-P}	Gap$_{H-L}$
$[Au_{13}(PPhMe_2)_{10}Cl_2]^{3+}$	271.4	278.8	291.6	230.5	231.1	2.14
$[Au_{13}(PMe_3)_{10}Cl_2]^{3+}$	272.4	278.6	292.4	229.8	230.1	2.06
$[Au_{13}(PH_3)_{10}Cl_2]^{3+}$	276.7	277.0	293.9	227.3	230.3	1.91
$[Au_{13}(PF_3)_{10}Cl_2]^{3+}$	278.8	276.4	295.6	224.5	226.9	1.56
$Au_{13}Cl_2^{3+}$	293.5	273.1	299.0	222.6		0.68
Au_{13}^{5+}	278.9	278.9	293.2			2.08

[a] Sequence number of Au atom is shown in Fig. 1

278.9 pm in Au_{13} and Au_{13}^{5+}, respectively. Thus, Au_{13}^{5+} is not thermodynamically stable, and possibly dissociates to smaller clusters or congregates with other clusters because of positive charges. Concerning the electron-deficient naked core, the ligand can donate electrons to the core and stabilize it. Another important point is that the ligand can protect the core from other cores and thus avoid congregating effects.

In the present study, we found different effects on cluster stability for the Cl^- and the PR_3 ligand. Traditional chemical bonding between ligand (Lewis base) and metal core (Lewis acid) is usually described in terms of donor–acceptor interactions between the occupied orbital of the donor and the vacant orbitals of the acceptor. The generally accepted bonding model, first suggested by Dewar [50] and later elaborated by Chatt and Duncanson [51], focuses on donor → acceptor σ donation and acceptor → donor π backdonation. For the Cl^- ligand, the major interaction involves the σ donation between the occupied $3p$ orbital of Cl^- and the vacant $8h_g$ orbitals of Au_{13}^{5+}. Unlike the traditional Dewar-Chatt-Duncanson (DCD) model, there is no acceptor → donor π backdonation because Cl^- has no vacant π orbital. On the other hand, the Cl^- ligand counteracts the positive charges of the core, reducing Coulomb repulsion. This phenomenon can be seen in the results presented in Table 4. The $R_{Au(1)-Au(5)}$ interaction is shortened from 278.9 to 273.1 pm by the action of Cl^-.

For the PR_3 ligand (here PH_3 is applied to illustrate the interaction), we investigated the energy-level correlation diagram of the frontier orbitals of $Au_{13}Cl_2^{3+}$, $(PH_3)_{10}$ and $[Au_{13}(PH_3)_{10}Cl_2]^{3+}$ in Fig. 3. As a typical DCD model, the major interaction occurs between the frontier orbitals of the gold core and the ligand. From the shape of the vacant orbital $15a_{1g}$ of $Au_{13}Cl_2^{3+}$ in Fig. 3, it is obvious that this orbital is the bonding orbital for Au(1)–Au(2) (having the same axes with Au–Cl) and the peripheral gold atoms. The core becomes more stable because the peripheral gold atoms are involved in effective chemical bonding via the action of $(PH_3)_{10}$. Certainly, the Au(1)–Au(2) bond also becomes stronger, as confirmed by the data given in Table 4. The $R_{Au(1)-Au(2)}$ bond is shortened from 293.5 to 271.4 pm, and the $R_{Au(4)-Au(5)}$ bond is shortened from 299.0 to 291.6 pm. Thus the primary reason underlying

cluster stability is that the Au(1)–Au(2) and Au(4)–Au(5) bonds are strengthened by the action of the PR_3 ligand.

$[Au_{13}(PR_3)_{10}Cl_2]^{3+}$ (R_3 = Me2Ph, Me$_3$, H$_3$, I$_3$, Br$_3$, Cl$_3$, F$_3$)—differences in the ligands

We next investigated the kind of ligand that can best stabilize the gold core? Several PR_3 ligands (R = Me, H, F, Cl, Br, I) with obvious differences in their capabilities as electron donors were compared. The main geometric parameters of $[Au_{13}(PR_3)_{10}Cl_2]^{3+}$ (R_3 = Me$_2$Ph, Me$_3$, H$_3$, F$_3$) are shown in Table 4. The change in each parameter is well matched to the electron donor ability of the ligand. As shown in Fig. 3b, the vacant orbital $15a_{1g}$ is the bonding orbital for $R_{Au(1)-Au(2)}$ and $R_{Au(4)-Au(5)}$ and the antibonding orbital for $R_{Au(1)-Au(5)}$ and R_{Au-Cl}. For the orbital action of the ligands, these bonds are shortened with bonding effect, and elongated with antibonding effect. As the electron donor ability of the ligand increases, more electrons enter the $15a_{1g}$ orbital. Then, the $R_{Au(1)-Au(2)}$ and $R_{Au(4)-Au(5)}$ bonds are shortened gradually with the bonding effect. Conversely, the bond lengths of $R_{Au(1)-Au(5)}$ and R_{Au-Cl} increase gradually with the antibonding effect.
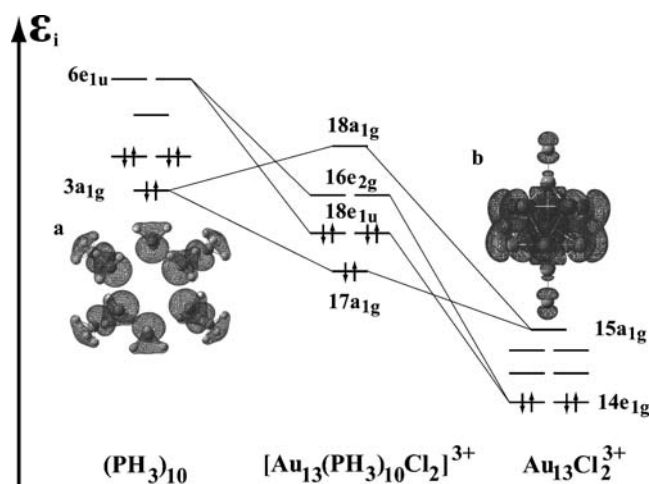

Fig. 3 Orbital correlation diagrams of $(PH_3)_{10}$, $Au_{13}Cl_2^{3+}$ and $[Au_{13}(PH_3)_{10}Cl_2]^{3+}$. **a** The orbital shape of the $3a_{1g}$ of $(PH_3)_{10}$; **b** the orbital shape of the $15a_{1g}$ of $Au_{13}Cl_2^{3+}$

Table 5 Bond energy analysis between $Au_{13}Cl_2^{3+}$ and $(PR_3)_{10}$ in $[Au_{13}(PR_3)_{10}Cl_2]^{3+}$ (R = Me, H, F, Cl , Br) . Values are in kcal mol^{-1}

	PMe$_3$	PH$_3$	PI$_3$	PBr$_3$	PCl$_3$	PF$_3$
ΔE_{prep}	46.4	26.8	41.7	43.6	31.2	37.0
ΔE_{int}	−706.2	−528.4	−438.2	−424.4	−418.7	−405.2
ΔE_{pauli}	1,762.3	1,605.3	1,073.1	1,347.9	1,509.6	1,624.9
ΔE_{elstat} [a]	−1,578.6 (64.0%)	−1,344.0 (63.0%)	−713.8 (47.2%)	−951.1 (53.7%)	−1,099.7 (57.0%)	−1,208.7 (59.5%)
ΔE_{orb} [a]	−889.9 (36.0%)	−789.7 (37.0%)	−797.6 (52.8%)	−821.2 (46.3%)	−828.6 (43.0%)	−821.4 (40.5%)
ΔE_{σ} [b]	−694.1 (78.0%)	−604.9 (76.6%)	−548.0 (68.7%)	−563.3 (68.6%)	−570.1 (68.8%)	−576.6 (70.2%)
ΔE_{π} [b]	−195.8 (22.0%)	−184.8 (23.4%)	−249.6 (31.3%)	−257.9 (31.4%)	−258.5 (31.2%)	−244.8 (29.8%)
ΔE_{b}	−659.8	−501.6	−396.5	−380.8	−387.5	−368.2

[a] Value in parentheses give the percentage of attractive interactions $\Delta E_{elstat} + \Delta E_{orb}$

[b] Value in parentheses give the percentage of orbital interactions ΔE_{orb}

Table 5 shows the results of bond EDA [52–54]. The standard definition of the bond energy ΔE_b between two fragments A and B is

$$\Delta E_b = E_{AB} - E_A - E_B \qquad (1)$$

Within the EDA method, the bond energy between the two fragments $Au_{13}Cl_2^{3+}$ and $(PR_3)_{10}$ is decomposed into two contributions:

$$\Delta E_b = \Delta E_{prep} + \Delta E_{int} \qquad (2)$$

ΔE_{prep} is the energy change of fragments A and B from isolated equilibrium structure to the structure in compound A–B. ΔE_{int} is the interaction energy between the two fragments in the molecule; ΔE_{int} can be further divided into three main components:

$$\Delta E_{int} = \Delta E_{pauli} + \Delta E_{elstat} + \Delta E_{orb} \qquad (3)$$

ΔE_{pauli} gives the repulsive interaction between the overlapping fragments in the molecule caused by the fact that two electrons of the same spin cannot occupy the same region in space. ΔE_{elstat} gives the electrostatic interaction of the electron density distributions of the fragments. Finally, the orbital interaction term ΔE_{orb} represents the stabilization produced when the fragment orbital and electron densities are allowed to relax to the molecular equilibrium situation.

As shown in Table 5, ΔE_{prep} has little proportion in all energy terms because there is no obvious distortion of ligands to form the complex. Figure 4 shows the correlation between ΔE_{int} and the Pauling electronegativities of the R substituents. It can be concluded that ΔE_{int} increases as the electronegativity of the R substituents increases. The largest contribution to ΔE_{int} values for all complexes is the repulsive term ΔE_{pauli}, which derives from the overlap repulsion of the P lone-pair and the Au closed core shells. The value of ΔE_{pauli} is related to the scale of the ligand and

the R_{Au-P}. The value of ΔE_{pauli} is largest for the $[Au_{13}(PMe_3)_{10}Cl_2]^{3+}$ complex because this has the biggest PMe$_3$ ligand. ΔE_{pauli} is overcompensated by electrostatic and orbital interaction attractions, with negative values of ΔE_{elstat} and ΔE_{orb}. The fact that ΔE_{elstat} values are greater than ΔE_{orb} values for all complexes suggests that the P–Au bonds are more electrostatic than covalent in character. Also, the proportion of ΔE_{int} contributed by ΔE_{elstat} increases gradually from PI$_3$ to PMe$_3$, suggesting that the interaction between the gold core and ligand tends to be more electrostatic when the ligand has a strong ability to donate electrons.

The structure of the gold core with one PR$_3$ ligand has C_s symmetry, which gives only a′ and a″ symmetries. One component of the near-degenerate Au$_{13}$Cl$_2$–PR$_3$ π-orbital belongs to a″, the other to a′, which is also symmetrical to the σ-orbital. Therefore, we can define the σ and π contributions as follows: $\Delta E_{\pi} = 2\Delta E_{orb}(a'')$ and $\Delta E_{\sigma} = \Delta E_{orb}(a') - \Delta E_{orb}(a'')$. The final values of the ΔE_{σ} and ΔE_{π} terms are gained by the gradual addition of ten PR$_3$ ligands. The proportion of ΔE_{σ} in ΔE_{orb} has the sequence of different ligands: PMe$_3$ > PH$_3$ > PF$_3 \approx$ PCl$_3 \approx$ PBr$_3 \approx$ PI$_3$. This series indicates that the σ donor proportion in

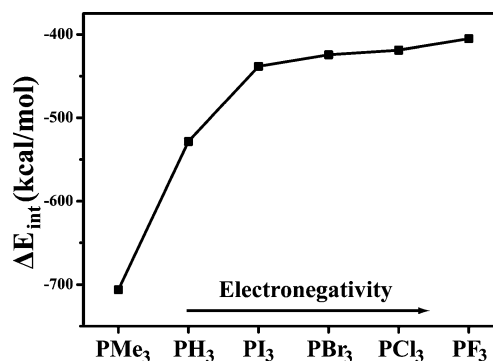**Fig. 4** Relationship of ΔE_{int} between $Au_{13}Cl_2^{3+}$ and $(PR_3)_{10}$ ligands expressed as the Pauling electronegativity of PR$_3$

orbital interaction between the core and the ligand increases with the strength of the electron donor. This strong electron donor capacity is the reason that PH_3 is a better ligand than other ligands such as NH_3. This result is corroborated by the computed results in a study by Brinck et al. [55], who showed that PH_3 electrons are more reactive than those of NH_3. The sequence is also in agreement with the work of Branchadell et al. [56], which classified the phosphanes into three groups: PMe_3, PPh_3, and $P(i\text{-}Pr)_3$ were considered as σ-donor ligands, PH_3 and $P(OMe)_3$ as intermediate cases, and PF_3 and $P(NC_4H_4)_3$ as σ-donor/π-acceptor ligands. Concerning the ΔE_b term, the sequence of different ligands is $PMe_3 > PH_3 > PI_3 > PBr_3 \approx PCl_3 > PF_3$. Just this rule was found by our recent work [57], which suggests that an σ-donor ligand, having a positive charge, is more appropriate to protect the gold core.

Summary and conclusions

The present work investigated some phosphane-stabilized gold clusters $[Au_{13}(PR_3)_{10}Cl_2]^{3+}$ (PR_3 = PMe_2Ph, PMe_3, PH_3, PF_3, PCl_3, PBr_3, PI_3) using several ab-initio and DF methods. The follow conclusions about the stability of gold clusters can be drawn from the results:

1. Five factors influence the stability of the metal core: (1) compact, symmetrical geometry; (2) particularly efficient radial bonding; (3) a filled spherical electronic shell and large energy gap to vacant orbital; (4) aurophilic attraction in the periphery; and (5) strong relativistic effects. Most known metal cores, such as WAu_{12}, $AlPb_{12}^+$, and $ZnGe_{12}$, exhibit all of these factors.

2. Protection by ligands plays an important role in the stability of gold clusters. In addition, the interaction between the ligand and the gold core is the key to understanding the extraordinary stability of these clusters. Different kinds of ligands make different contributions to stabilizing the clusters. In this study, the Cl^- ligand was found to counteract the positive charge of the gold core, and the PR_3 ligand coordinates to the core surface by dative bonds as a weak Lewis base. Conforming to a traditional DCD model, the interaction between the PR_3 ligand and the gold core can be divided into σ-donor and π-backdonor, with the σ-donor acting as a key factor in the stability of the cluster. In detail, the PR_3 ligand shorten the $R_{Au(1)-Au(2)}$ and $R_{Au(4)-Au(5)}$ bonds, clearly stabilizing the gold core.

3. There are two important points to remember when considering which kind of ligand should be chosen to protect the gold core: (1) the ligand should be a good electron donor; (2) the ligand can be very effective in protecting the gold core from aggregating effects.

Certainly, there is particularly good stabilization if the ligand can coordinate to the metal core as a chelated motif.

References

1. Fan H, Yang K, Boye DM, Sigmon T, Malloy KJ, Xu H, López GP, Brinker CJ (2004) Science 304:567–571
2. Zheng N, Stucky GD (2006) J Am Chem Soc 128:14278–14280
3. Wohltjen H, Snow AW (1998) Anal Chem 70:2856–2859
4. Negishi Y, Tsunoyama H, Suzuki M, Kawamura N, Matsushita MM, Maruyama K, Sugawara T, Yokoyama T, Tskuda T (2006) J Am Chem Soc 128:12034–12035
5. Shaw CF III (1999) Chem Rev 99:2589–2600
6. Bartiett PA, Bauer B, Singer SJ (1978) J Am Chem Soc 100:5085–5089
7. Woehrle GH, Warner MG, Hutchison JE (2002) J Phys Chem B 106:9979–9981
8. Yanagimoto Y, Negishi Y, Fujihara H, Tsukuda T (2006) J Phys Chem B 110:11611–11614
9. Briant CE, Theobald BRC, White JW, Bell LK, Mingos DMP, Welch AJ (1981) J Chem Soc Chem Commun 201–202
10. Zhang HF, Stender M, Zhang R, Wang C, Li J, Wang LS (2004) J Phys Chem B 108:12259–12263
11. Teo BK, Shi X, Zhang H (1992) J Am Chem Soc 114:2743–2745
12. Schmid G, Pfeil R, Boese R, Bandermann F, Meyer S, Calis GHM, van der Velden JWA (1981) Chem Ber 114:3634–3642
13. Garzón IL, Posada-Amarillas A (1996) Phys Rev B 54:11796–11802
14. Guliamov O, Frenkel AI, Menard LD, Nuzzo RG, Kronik L (2007) J Am Chem Soc 129:10978–10979
15. Larsson JA, Nolan M, Greer JC (2002) J Phys Chem B 106:5931–5937
16. Häkkinen H, Barnett RN, Landman U (1999) Phys Rev Lett 82:3264–3267
17. Zhu MZ, Aikens CM, Hollander FJ, Schatz GC, Jin RC (2008) J Am Chem Soc 130:5883–5885
18. Pei Y, Gao Y, Zeng XC (2008) J Am Chem Soc 130:7830–7832
19. Iwasa T, Nobusada KJ (2007) Phys Chem C 111:45–49
20. Li X, Kiran B, Li J, Zhai HJ, Wang LS (2002) Angew Chem Int Ed 41:4786–4789
21. Neukermans S, Janssens E, Chen ZF, Silverans RE, Schleyer PvR, Lievens P (2004) Phys Rev Lett 92:163401–163404
22. Cui LF, Huang X, Wang LM, Li J, Wang LS (2007) Angew Chem Int Ed 46:742–745
23. Pyykkö P, Runeberg N (2002) Angew Chem Int Ed 41:2174–2176
24. Kumar V, Kawazoe Y (2002) Appl Phys Lett 80:859–861
25. Long J, Qiu YX, Chen XY, Wang SG (2008) J Phys Chem A 112:12646–12652
26. Furuse S, Koyasu K, Atobe J, Nakajima A (2008) J Chem Phys 129:064311–064316
27. Wang LM, Bulusu S, Zhai HJ, Zeng XC, Wang LS (2007) Angew Chem Int Ed 46:2915–2918
28. Walter M, Akola J, Lopez-Acevedo O, Jadzinsky PD, Calero G, Ackerson CJ, Whetten RL, Grönbeck H, Häkkinen H (2008) Proc Natl Acad Sci USA 105:9157–9162
29. Hirsch A, Chen ZF, Jiao HJ (2000) Angew Chem Int Ed 39:3915–3917

30. Pyykkö P (1997) Chem Rev 97:597–636
31. Pyykkö P, Tamm T (1998) Organometallics 17:4842–4852
32. Pyykkö P (1988) Chem Rev 88:563–594
33. TURBOMOLE, Version 5.10; Quantum Chemistry Group, University of Karlsruhe: Karlsruhe, Germany
34. Te Velde G, Bickelhaupt FM, Baerends EJ, Guerra CF, Van Gisbergen SJA, Snijders JG, Ziegler T (2001) J Comput Chem 22:931–967
35. Slater JC (1951) Phys Rev 81:385–390
36. Vosko SH, Wilk L, Nusair M (1980) Can J Phys 58:1200–1211
37. Becke AD (1988) J Chem Phys 88:2547–2553
38. Perdew JP (1986) Phys Rev B 34:7406
39. Perdew JP, Burke K, Ernzerhof M (1996) Phys Rev Let 77:3865–3868
40. Stephens PJ, Devlin FJ, Chabalowski CF, Frisch MJ (1994) J Phys Chem 98:11623–11627
41. Becke AD (1993) J Chem Phys 98:5648–5652
42. Andrae D, Häupermann U, Dolg M, Stoll H, Preup H (1990) Theor Chem Acta 77:123–141
43. Gunnarsson O, Lundqvist BI, Wilkins JW (1974) Phys Rev B 10:1319–1327
44. Perdew JP, Wang Y (1992) Phys Rev B 45:13244–13249
45. Van Lenthe E, Baerends EJ, Snijders JG (1993) J Chem Phys 99:4597–4610
46. Rosén A, Lindgren I (1968) Phys Rev 176:114–125
47. Dewar MJS (1951) Bull Soc Chim Fr 18:C71–C79
48. Ditchfield R, Hehre WJ, Pople JA (1971) J Chem Phys 54:724–728
49. Frisch MJ, Trucks GW, Schlegel HB, Scuseria GE, Robb MA, Cheeseman JR, Montgomery JA Jr, Vreven T, Kudin KN, Burant JC, Millam JM, Iyengar SS, Tomasi J, Barone V, Mennucci B, Cossi M, Scalmani G, Rega N, Petersson GA, Nakatsuji H, Hada M, Ehara M, Toyota K, Fukuda R, Hasegawa J, Ishida M, Nakajima T, Honda Y, Kitao O, Nakai H, Klene M, Li X, Knox JE, Hratchian HP, Cross JB, Bakken V, Adamo C, Jaramillo J, Gomperts R, Stratmann RE, Yazyev O, Austin AJ, Cammi R, Pomelli C, Ochterski JW, Ayala PY, Morokuma K, Voth GA, Salvador P, Dannenberg JJ, Zakrzewski VG, Dapprich S, Daniels AD, Strain MC, Farkas O, Malick DK, Rabuck AD, Raghavachari K, Foresman JB, Ortiz JV, Cui Q, Baboul AG, Clifford S, Cioslowski J, Stefanov BB, Liu G, Liashenko A, Piskorz P, Komaromi I, Martin RL, Fox DJ, Keith T, Al-Laham MA, Peng CY, Nanayakkara A, Challacombe M, Gill PMW, Johnson B, Chen W, Wong MW, Gonzalez C, Pople JA (2003) Gaussian 03, Revision B3. Gaussian Inc, Pittsburgh, PA
50. Chatt J, Duncanson LA (1953) J Chem Soc 2929–2947
51. Kitaura K, Morokuma K (1976) Int J Quantum Chem 10:325–340
52. Morokuma J (1971) J Chem Phys 55:1236–1244
53. Uddin J, Frenking G (2001) J Am Chem Soc 123:1683–1693
54. Lein M, Frunzke J, Timoshkin A, Frenking G (2001) Chem Eur J 7:4155–4163
55. Brinck T, Murray JS, Politzer P (1993) Int J Quantum Chem 48:73–88
56. González-Blanco Ò, Branchadell V (1997) Organometallics 16:5556–5562
57. Li J, Qiu YX, Wang SG (2009) J Phys Chem A 113:1646–1652
58. Bishea GA, Morse MD (1991) J Chem Phys 95:5646–5659
59. Wesendrup R, Hunt T, Schwerdtfeger P (2000) J Chem Phys 112:9356–9362
60. Huber KP, Herzberge G (1979) Molecular spectra and molecular structure. IV. Constants of diatomic molecules. Van Nostrand, New York